

Article

The Influence of O₂ on Decomposition Characteristics of c-C₄F₈/N₂ Environmental Friendly Insulating Gas

Song Xiao ¹, Shuangshuang Tian ^{1,2,*}, Xiaoxing Zhang ^{1,*} , Yann Cressault ² , Ju Tang ¹, Zaitao Deng ¹ and Yi Li ¹ 

¹ School of Electrical Engineering, Wuhan University, BaYi Street No. 299, Wuhan 430072, China; xiaosongxs@gmail.com (S.X.); whtangju@whu.edu.cn (J.T.); 15172313258@163.com (Z.D.); liyi_whuee@163.com (Y.L.)

² LAPLACE (Laboratoire Plasma et Conversion d’Energie), UPS, INPT, Université de Toulouse, 118 route de Narbonne, F-31062 Toulouse CEDEX 9, France; yann.cressault@laplace.univ-tlse.fr

* Correspondence: tianshuang1002@yahoo.com (S.T.); xiaoxing.zhang@outlook.com (X.Z.); Tel.: +86-158-2757-4383 (S.T.); +86-136-2727-5072 (X.Z.)

Received: 5 August 2018; Accepted: 19 September 2018; Published: 29 September 2018



Abstract: The c-C₄F₈ gas is considered to have great potential as a gaseous medium for gas-insulated equipment, due to its good insulation properties and its relatively low greenhouse gas potential (GWP) relative to SF₆. However, the decomposition is an important indicator of its use in equipment. In this paper, the decomposition characteristics of c-C₄F₈ and the influence by oxygen have been explored through experiments and theoretical calculations. Firstly, the breakdown test of mixed gas was carried out and the precipitated elements of the electrodes and breakdown products of gas mixture were analyzed by X-ray photoelectron spectroscopy (XPS) and gas chromatography mass spectrometry (GC-MS). At the same time, the differences in decomposition products have also been studied when a small amount of O₂ was present. The path and mechanism of c-C₄F₈ decomposition is then discussed, based on density functional theory (DFT). The results show that the black powdery substance descends on the electrode surface after the breakdown of the mixture of c-C₄F₈/N₂ gas containing O₂, and its main constituent elements are C, O and F. O₂ can promote the decomposition of c-C₄F₈. The mixture with O₂ produced a large number of additional toxic and corrosive COF₂ in addition to generating more CF₄, C₂F₄, C₂F₆, C₃F₆ and C₃F₈. The GWP values of the products are lower than SF₆. Comprehensive insulation properties and decomposition characteristics, c-C₄F₈ should not be mixed with dry air for use, and the oxygen content should be strictly controlled in c-C₄F₈ mixed gas.

Keywords: SF₆ alternative gas; c-C₄F₈/N₂ gas mixture; breakdown characteristics; decomposed component; greenhouse effect

1. Introduction

Sulfur hexafluoride (SF₆) has been widely used in the power industry due to its excellent insulation and arc extinguishing properties. A total of 80% of the SF₆ is used in high voltage circuit breakers and other high-pressure gas insulation equipment [1]. However, SF₆ was listed as one of the six major greenhouse gases with a GWP (Global Warming Potential) of 23,500 and an atmospheric lifetime of 3200 years in the 1972 Kyoto Protocol [2,3]. Although the atmospheric concentration of SF₆ is relatively low, contributing to 0.1% of the total anthropogenic radiative forcing, the concentration is growing continuously because of the compound’s long lifetime of ~3200 years [4,5]. Over the past five years, the content of SF₆ in the global atmosphere has increased by 20% [6]. California proposed that the use of SF₆ in the electrical field should be reduced annually from 2020 and the European Union

plans to reduce SF₆ emissions to 2/3 between 2014 and 2030 [7]. In order to ensure the sustainable development of the power industry, reducing the use of SF₆ has become an important task in the current production and use of power equipment. In addition, SF₆ could generate a variety of harmful gases such as SO₂, SOF₂, SO₂F₂, S₂F₁₀, under partial discharge, spark discharge or arc discharge [8–10]. Therefore, looking for an environmentally friendly and safe gas as an alternative insulation medium in power equipment, has become a sought-after solution.

In the current research, the ideal substitutes for SF₆ include perfluorocarbons (PFCs), trifluoroiodomethane (CF₃I), and other gases. Among them, the C-I bond of CF₃I can easily be broken to produce iodine solid, which produces toxic gases such as CH₃I, COF₂ after discharge, which is not conducive to the long-term safe operation of the equipment [11,12]. Of course, the adsorbent can adsorb by-products, but finding a suitable adsorbent and whether the adsorbent has an effect on the insulation is also a problem. PFCs mainly include C₂F₆, C₃F₈, c-C₄F₈, among which c-C₄F₈ is the most excellent insulating property (about 1.18 times that of SF₆). It is non-toxic to humans and the environment with the GWP of 8700 and the liquefaction temperature of −6 °C [13]. Although c-C₄F₈ also has greenhouse effect, its global warming potential is much lower than SF₆ (23,000). Replacement of SF₆ with c-C₄F₈ in power equipment will significantly reduce the greenhouse effect. So far, there are still many scholars to study the possibility of replacement SF₆.

Concerning the new environmentally friendly insulation gas produced by 3M, apart from the C₅F₁₀O (Novac 5110) mentioned by reviewers, there is also C₄F₇N (Novac 4710) [14,15]. Both of these gases are hot in the current stage of research. We do not deny the superior performance of these two gases. However, gas liquefaction temperatures such as C₅F₁₀O are too high to be suitable for all types of gas-insulated equipment. In recent years, many researchers have studied the insulation performance of c-C₄F₈ with N₂, CO₂ and other mixed gases under DC, AC and lightning impulse voltage. It is concluded that the electrical strength of c-C₄F₈-N₂ mixtures can only reach approximately 0.57 times that of pure SF₆ at 0.5 MPa with c-C₄F₈ concentrations of 20% [16], but 15–20% c-C₄F₈ gas mixture meets the requirements of electrical equipment, and mixtures can greatly reduce the impact of insulating gas on the environment [17–19]. Li et al. calculated the mixtures between c-C₄F₈ and variety of gases in order to determine the mixed gas insulation. For example, the critical breakdown strength of c-C₄F₈-N₂ and c-C₄F₈-air are similar and significantly higher than other mixed gases. When the content of c-C₄F₈ exceeds 80%, the insulation property of mixture can reach the level of pure SF₆ but there is a lack of experimental data for validation [20]. Some studies on the decomposition characteristics of c-C₄F₈ have achieved some results. Li et al. [21] explored the decomposition products of c-C₄F₈ under various typical faults based on the gas chromatograph-mass spectrometer test. It was found that the decomposition of c-C₄F₈ mainly produced CF₄, C₂F₆ and C₂F₄, C₃F₈, C₃F₆. Hayashi et al. [22] discussed the main pathways for the dissociation of c-C₄F₈ to generate free radicals CF₂ based on the density functional theory (DFT), providing guidance for further investigation of the decomposition mechanism of c-C₄F₈. As the core insulating gas, c-C₄F₈ may need to be mixed with other gases due to the liquefaction temperature, and dry air is the common buffer gas. The theoretical calculations and experimental studies have shown that c-C₄F₈-N₂ has good insulation properties. Potential alternative environmentally-friendly alternative gas and dry air often are mixed as an insulating medium. Additionally, in order to promote the recovery after the arc, O₂ often appears in the arc medium. However, the related research is lacking, and the toxicity and environmental safety of the decomposition products after mixing with oxygen are urgent to be investigated. Oxygen introduction is divided into passive introduction and active introduction. Passive introduction mainly refers to the introduction of trace amounts of oxygen introduced by the equipment during operations such as transportation, assembly, maintenance, and ventilation. Generally, it will not exceed 1%, which is similar to the problems faced by SF₆ gas insulation equipment [23]. The other is active introduction, because the environment-friendly insulation gas may be mixed with dry air to fill the equipment. In addition to nitrogen and CO₂, dry air mainly contains O₂. The safety of the other two gases has been verified in many studies [24]. Therefore, the influence of O₂ on the insulation performance and decomposition properties of c-C₄F₈ also needs to be studied, and it is very urgent.

The influence of oxygen on the decomposition of mixed gas can provide the basis for exploring $c\text{-C}_4\text{F}_8$ -air and the performance analysis of the decomposition products is also an important indicator of evaluation gas application. In order to obtain a new insulation formula for environmental safety and to study the possible causes of hazardous products, it is necessary to test and analyze the physical and chemical processes of oxygen gas mixture discharge.

In this paper, the decomposition products of pure $c\text{-C}_4\text{F}_8$ and the $c\text{-C}_4\text{F}_8/\text{N}_2$ mixed gas are explored experimentally and the influence of oxygen are also considered. N_2 is just the buffer gas added in order to reduce the liquefaction temperature, because its physical and chemical properties are stable and not easy to decompose. After several frequency breakdown experiments, the decomposition products and electrode precipitation elements were obtained by GC-MS (gas chromatography mass spectrometry) and XPS (X-ray photoelectron spectroscopy). Based on the density functional theory, the structural characteristics of $c\text{-C}_4\text{F}_8$ were calculated firstly, the stability of the molecular structure and the reactive sites were analyzed. The possible dissociation pathways of $c\text{-C}_4\text{F}_8$ and the formation mechanism of the decomposition products were discussed. The purpose of this paper is to study the changes of decomposition products with the participation of oxygen and explore the safety and environmental protection of products. The comprehensive evaluation of the influence of oxygen on the decomposition characteristics of $c\text{-C}_4\text{F}_8$ provides a reference for the research of SF_6 alternative gas.

2. Experimental Setup

The test was carried out at a 50 Hz AC voltage gas insulation performance test platform. In the experiment, N_2 , which is stable chemically gas, was used as the buffer gas.

Before the experiment, the airtightness of the gas chamber was checked, and the sealed gas chamber was evacuated using a vacuum pump (BECKER/VT4.16, BECKER, Wuppertal, Germany) and was allowed to stand still for 60 min (less than 10 Pa). N_2 gas is used to clean the gas chamber. The above steps are repeated 2 to 3 times in order to avoid the influence of impurity gases. After cleaning, the mixed gas is introduced into the gas chamber. The ball-ball electrode was used in the experiment. The diameter of the copper ball was 50 mm with the electrode spacing of 5 mm. The range of applications for mixed gases may be medium-voltage gas-insulated devices such as switch cabinets. Because the key part of the conductivity in these devices is made of copper, it is used as the electrode material. The purity level of the $c\text{-C}_4\text{F}_8$ and N_2 is 99.999%.

According to the literature [24], it has been shown that the breakdown behavior of $c\text{-C}_4\text{F}_8/\text{N}_2$ mixture (the mixing ratio of $c\text{-C}_4\text{F}_8$ is 5%~20%) under uniform electric field is similar to that of SF_6/N_2 with the same mixing ratio. The Corona discharge performance of $c\text{-C}_4\text{F}_8/\text{N}_2$ is better than the same mixing ratio SF_6/N_2 . If the $c\text{-C}_4\text{F}_8/\text{N}_2$ gas mixture is not liquefied at $-30\text{ }^\circ\text{C}$, the content of $c\text{-C}_4\text{F}_8$ in the gas mixture is at most about 15% [25]. Therefore, the pure $c\text{-C}_4\text{F}_8$, 15% $c\text{-C}_4\text{F}_8/\text{N}_2$ and with 3% O_2 were selected as samples in this paper. The test was carried out by a step-and-step method, and the gas mixture was broken down 50 times to detect decomposition products. The details are shown in Figure 1.

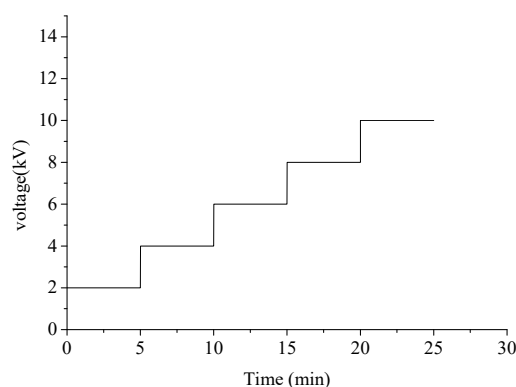


Figure 1. The step method.

GC-MS is used for detection of gas mixture components after the breakdown discharge. CP Sil 5CB was selected as the column. GC analysis, the high purity He (the purity of gas is above 99.999%) gas is used as a carrier gas, and carrier gas filters (including He filter and RP oil filter) are used to filter out the impurities, which may affect the column and interfere with the experimental results. Inlet temperature is 220 °C and inlet pressure is 56.1 kPa. The injection mode uses a split flow method with a split ratio of 10:1 and an injection volume of 1 mL. The column flow rate is 1.2 mL/min, and the purge flow rate is 3.0 mL/min. The heating rate of gas into the oven is shown in Figure 2. The oven had an initial temperature of 35 °C, a final temperature of 150 °C, and a temperature increase rate of 40 °C/min. The column temperature was maintained at 35 °C for 0~8 min, and after 8 min, the temperature rose steadily to 150 °C, and the temperature rising rate was kept at 40 °C/min. MS analysis, the ion source temperature is 200 °C, the chromatographic mass spectrometry interface temperature is 220 °C, ionization mode is Electronic ionization (EI). The solvent delay time was 0.1 min; the detector voltage threshold was 100 and the voltage was 0.1 kV. The specific steps can be found in [26–30].

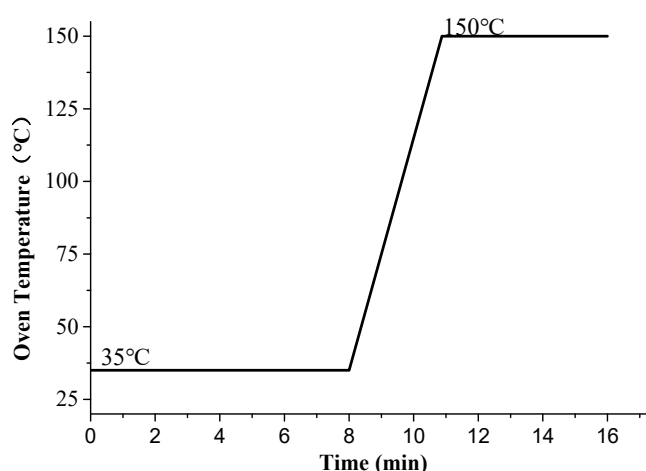


Figure 2. Oven temperature of GC-MS (gas chromatography mass spectrometry).

3. Experimental Results

3.1. Electrode Precipitate Component Analysis

Figure 3 shows the surface of the ball electrode before and after breakdown of pure $c\text{-C}_4\text{F}_8$, $c\text{-C}_4\text{F}_8/\text{N}_2$ gas without O_2 and with 3% O_2 . It can be seen that the surface of the copper ball electrode is covered with a layer of black powdery solid. Compared to pure gas, the mixed gas deposits are significantly less. However, the addition of oxygen increases the production of solid products while there only was a clear trace of ablation on the electrode surface at absence of O_2 in mixture. The ESCALAB 250Xi photoelectron spectrometer (Thermo Scientific Corp., Waltham, MA, USA) was used to scan the black surface of the electrode by XPS. It was found that it consisted of C, F, O and N elements. Table 1 shows the content of each component in the black material, in which the C content is 58.44%, which is the main constituent element, the content of O is 17.32%, the N element content is 0.75% and the F element content is 23.49%. Figure 4 shows the C photoelectron scanning.

Table 1. Element content of precipitates on spherical electrode surface.

Element	Concentration (%) (Precision: 0.01%)
C1s	58.44
O1s	17.32
N1s	0.75
F1s	23.49

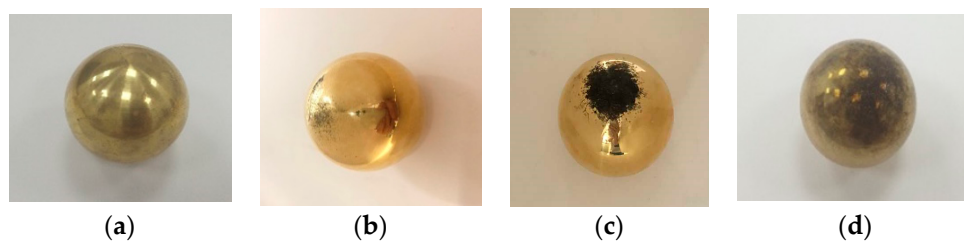


Figure 3. The spherical electrode before and after breakdown of $c\text{-C}_4\text{F}_8/\text{N}_2$ gas. (a) the ball electrode before breakdown; (b) 15% $c\text{-C}_4\text{F}_8/85\% \text{N}_2$; (c) 100% $c\text{-C}_4\text{F}_8$; (d) 15% $c\text{-C}_4\text{F}_8/82\% \text{N}_2/3\% \text{O}_2$.

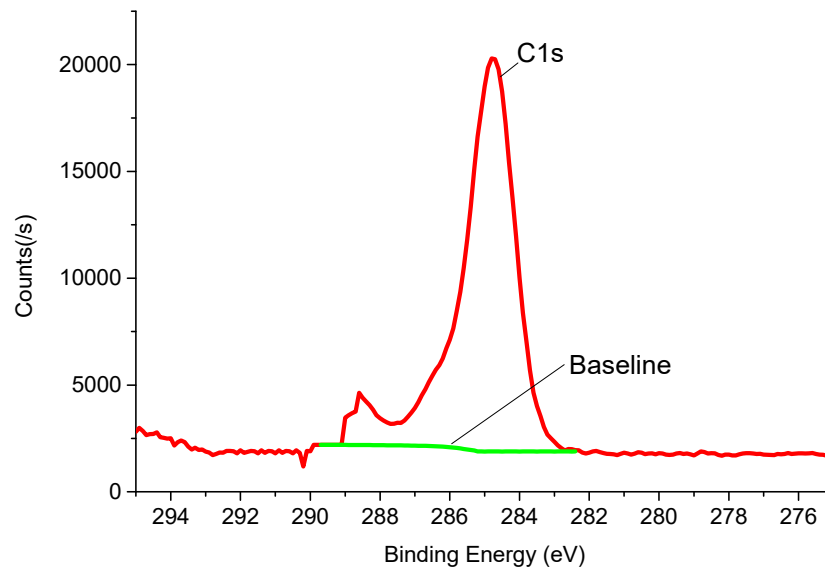


Figure 4. C element photoelectron scanning.

As shown in Figure 4, the maximum intensity of the corresponding C element binding energy is about 285 eV, corresponding to the chemical structure of the C–C single bond structure, which constitutes the C elemental elements. With C element loss of electrons, the binding energy can increase to 290 eV, corresponding to the chemical structure of O–C=O, which may constitute a variety of carbon oxides. Through XPS analysis, the black surface of the electrode may show a single element of C and various oxyfluorides of carbon. The test results are consistent with the literature [21].

3.2. Experimental Analysis of the Decomposition Products of $c\text{-C}_4\text{F}_8$ under Micro-Oxygen Condition

In order to further verify the accuracy of the experimental results, the gas-insulated test platform was used to conduct continuous, 50 rounds of pure $c\text{-C}_4\text{F}_8$, $c\text{-C}_4\text{F}_8/\text{N}_2$ mixed gas with 0% and 3% O_2 content breakdown tests and analysis of discharge breakdown components. The breakdown test was conducted on the mixed gas and the decomposition components of the mixed gas were detected. Figure 5a,b shows the GC-MS chromatograms (Varian Medical Systems, Inc., Palo Alto, CA, USA) of the two mixed gases after breakdown. Qualitative analysis is carried out using the combined methods of the United States National Institute of Standards and Technology (Nist14.0) database, and standard gas chromatography scanning.

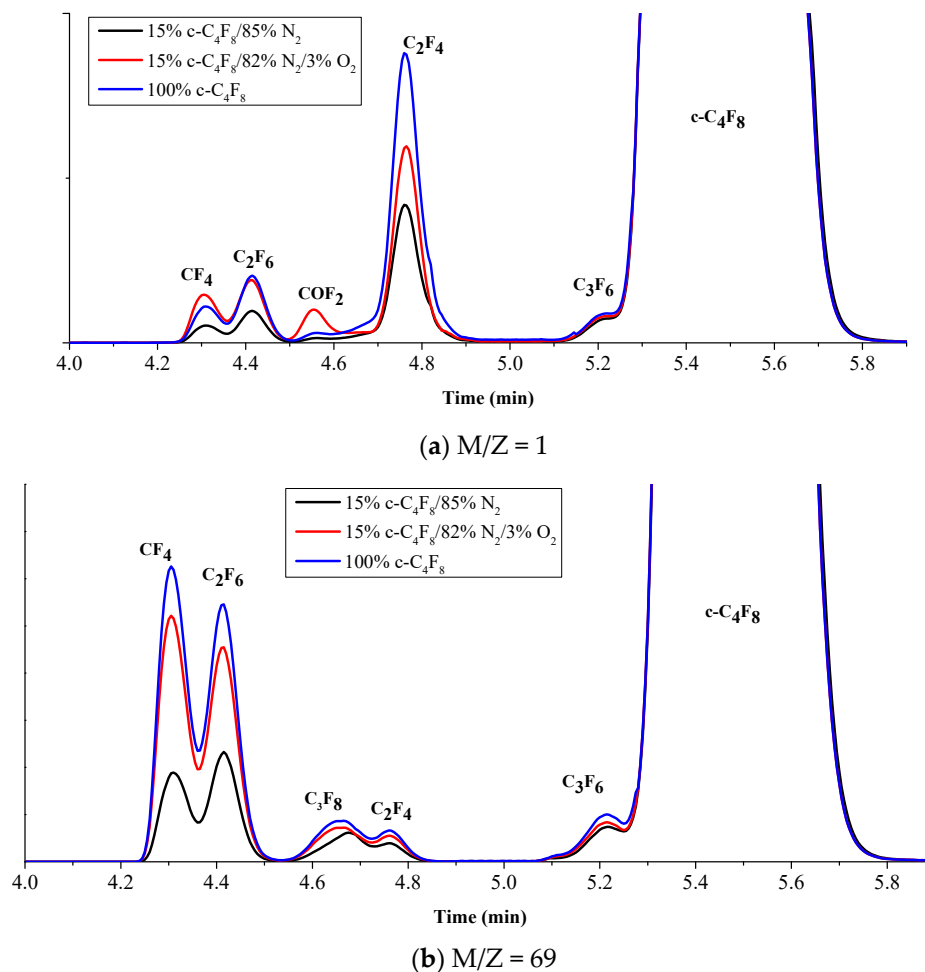


Figure 5. Chromatogram analysis of GC-MS (The ordinate indicates the relative peak intensity).

The mass-to-charge ratio $M/Z = 1$ was selected as the base peak. As shown in Figure 5a, the chromatograms of the two mixed gases showed the characteristic peaks of CF_4 , C_2F_6 , C_2F_4 and C_3F_6 . The characteristic peak of COF_2 also appears with O_2 of 3%. COF_2 is a highly toxic gas with a strong irritating effect on the skin and respiratory mucosa. It is also corrosive and can irreversibly damage equipment insulation. In order to display all products containing $CF_3\cdot$ groups, the results of the scan were analyzed using $M/Z = 69$ as the base peak, as shown in Figure 5b. Chromatogram in addition to CF_4 , C_2F_6 , C_2F_4 , C_3F_6 , C_3F_8 also appeared characteristic peaks. From the test results, the main decomposition products are from the $c-C_4F_8$ molecules, and N_2 in the mixed gas did not participate in the chemical reaction.

Test results show that pure gas is more likely to decompose and the intensity of each decomposition product monitored was higher than that of $c-C_4F_8/N_2$. In order to investigate the effect of O_2 on the decomposition of $c-C_4F_8/N_2$ gas mixture in more detail, Table 2 shows the peak intensities of the decomposition components of $c-C_4F_8/N_2$ gas mixture at 0% and 3% O_2 . It can be seen that with the addition of O_2 , the peak intensities of CF_4 , C_2F_6 , C_3F_8 and C_2F_4 all have large changes, and the peak intensity of CF_4 produced by $c-C_4F_8/N_2$ with 3% O_2 increased by 275.34%, C_2F_6 relative increase of about 200%, C_2F_4 and C_3F_8 relative growth of about 140%. The growth rate of CF_4 and C_2F_6 is higher than that of C_3F_8 . The above analysis shows that the decomposition of $c-C_4F_8$ is more likely to produce small molecule products and the mixed gas containing O_2 generates extra COF_2 . The presence of O_2 promotes the decomposition of $c-C_4F_8/N_2$.

Table 2. Peak strength of c-C₄F₈/N₂ mixed gas decomposition products under different O₂ contents.

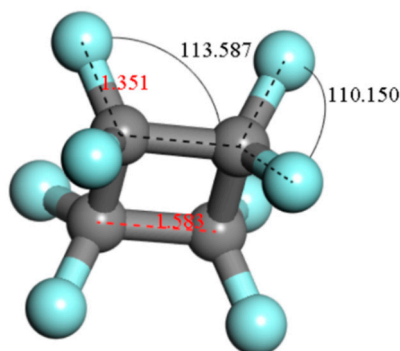
Products	0% O ₂	3% O ₂	The Growth Rate (%)
CF ₄	1,052,859	2,898,954	275.34
C ₂ F ₆	1,944,746	3,808,650	195.84
C ₃ F ₈	196,263	275,746	140.50
C ₂ F ₄	8,377,435	11,928,574	142.39
C ₃ F ₆	1,479,519	1,627,829	110.02

4. Discussion

In order to explore the discharge decomposition path of c-C₄F₈ and the effect of O₂ on its decomposition, a thermodynamic and kinetic combination method was used to analyze the orientation and mechanism of the reaction based on density functional theory (DFT). With regard to theoretical knowledge of calculations, it has been described in detail in our previous work [30,31]. The Dmol3 package was used to process exchange-related interactions using a local density approximation (LDA-PWC) approach to optimize the structure of c-C₄F₈ and O₂ [25]. To model the possible reaction path, the stable molecular configuration with the lowest energy is needed for selection. By calculating the energy of reactants and products, we can get the energy change before and after the reaction, and judge the difficulty of the reaction from the thermodynamic point of view. In addition, the constructed non-decomposing reaction path needs to be searched for transition state [32]. Because during the process of chemical bond breaking and rearrangement, the intermediate activated complexes will be absorbed by the reactants to produce a certain amount of energy, and the process of generating activated complexes often determines the reaction rate. Therefore, the transition state structure and the corresponding activation energy are helpful to evaluate the reaction from the kinetic point of view. Finally, combined with the test results, the dynamic equilibrium process of particles during the decomposition of c-C₄F₈ with O₂ was analyzed.

4.1. The Basic Properties of c-C₄F₈

Figure 6 shows the geometry of optimized c-C₄F₈ molecule structure, where the bond length is Å and the bond angle is °. The c-C₄F₈ molecule has a high degree of symmetry. The C-C bond length is 1.583 Å and the C-F bond length is 1.350 Å. The F-C-F bond angle is 110.150° and the F-C-C bond angle is 113.587°.

**Figure 6.** Molecular structure of c-C₄F₈.

The bond level is a physical quantity that describes the bond strength between adjacent atoms in the molecule, indicating the relative strength of the bond. In the collision of electrons and other particles or under high temperature conditions, the chemical bond may be broken, wherein the strength of the chemical bond relative to the strength of the smaller chemical bonds more difficult to break. Figure 7 shows the calculated chemical bond levels for the c-C₄F₈ and SF₆ molecules. According to the calculation results, the C-C bond in the c-C₄F₈ molecule has a bond level value of 0.924 and the C-F

bond with a value of 0.896. The intensity of the C-F bond in the $c\text{-C}_4\text{F}_8$ molecule is weaker than that of the C-C bond. Therefore, the C-F bond is more likely to dissociate than the C-C bond. In the SF_6 molecule, the S-F bond level value of the four co-planar F atoms and the S atom is 0.826, and the other two S-F bond level values are 0.829. Overall, the bond level of the chemical bonds in the SF_6 molecule is smaller than the bond order of the chemical bonds in the $c\text{-C}_4\text{F}_8$ molecule, indicating that the stability of the molecular structure of the SF_6 is inferior to that of the $c\text{-C}_4\text{F}_8$ molecule, which explains the $c\text{-C}_4\text{F}_8$ gas dielectric strength is superior to SF_6 gas.

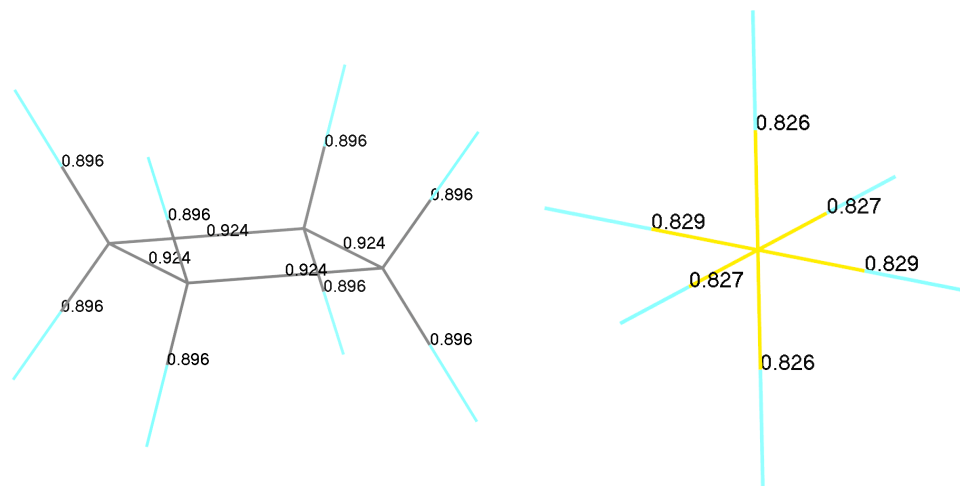
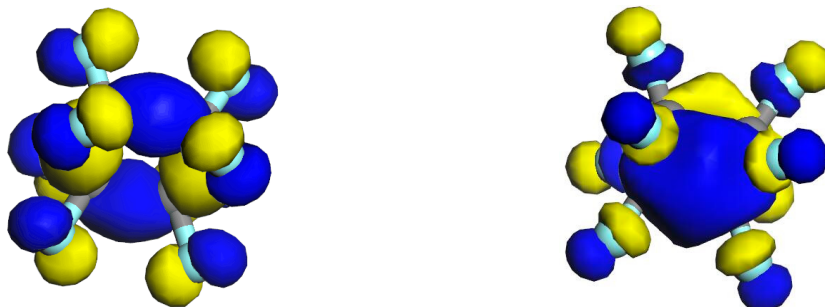


Figure 7. $c\text{-C}_4\text{F}_8$ and SF_6 bond-level distribution.

The distribution of the highest occupied molecular orbital (HOMO) and the lowest unoccupied molecular orbital (LUMO) of $c\text{-C}_4\text{F}_8$ is calculated from the orbital distribution of the molecules, as shown in Figure 8. The corresponding energies are -0.298645 Ha and -0.086768 Ha, respectively. The energy difference between LUMO and HOMO characterizes the stability of the gas involved in the chemical reaction. The larger the difference is, the larger the energy required for the electron transition in the molecule is and the more stable the molecule is.



HOMO (highest occupied molecular orbital) LUMO (lowest unoccupied molecular orbital)

Figure 8. $c\text{-C}_4\text{F}_8$ molecular orbital distribution.

4.2. The Decomposition Path of $c\text{-C}_4\text{F}_8$ and the Main Product Generation Mechanism

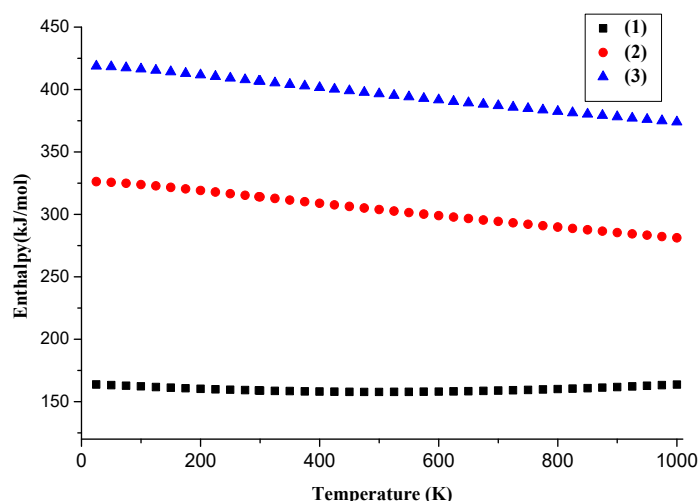
Electrons are the main factors that cause collision ionization and dissociation in the electric field. Under the high-energy electric field or local overheating, the chemical bonds in the molecular structure of $c\text{-C}_4\text{F}_8$ will be cleaved, generating various types of free radicals, thereby damaging the insulation structure. In combination with the molecular structure of $c\text{-C}_4\text{F}_8$, Table 3 shows the major pathways for the decomposition during the discharge process.

Table 3. c-C₄F₈ discharge decomposition path.

Pathway	Chemical Equation	Reaction Energy (kJ/mol)
(1)	c-C ₄ F ₈ → C ₂ F ₄ · + C ₂ F ₄ ·	173.8539
(2)	c-C ₄ F ₈ → C ₃ F ₆ · + CF ₂ ·	342.3815
(3)	c-C ₄ F ₈ → C ₄ F ₇ · + F·	434.8436

The decomposition pathway (1) refers to the process of two C-C bonds that located at the relative positions of the c-C₄F₈ molecule being disconnected to form free radicals. The pathway (2) refers to the disconnecting process of C-C bonds which are adjacent in the C-C₄F₈ molecule. The absorption energy required for pathway (1) is 173.8539 kJ/mol, which is lower than the 342.3815 kJ/mol required for pathway (2). The pathway (3) refers to the process of c-C₄F₈ which cleaves the C-F bond to produce C₄F₇· and F· free radicals, and the process need to absorb energy of 434.8436 kJ/mol, higher than pathway (1) and pathway (2).

Figure 9 shows the change trend of reaction energy of three decomposition paths (in Table 3) with temperature. As the temperature increases, the energy required for molecular decomposition decreases gradually, and the increase of temperature is in favor of the reaction. The effect of temperature is considered mainly because the temperature changes during the discharge. In particular, there will be a significant increase in the temperature at the moment of breakdown, and the temperature at the center of the breakdown arc may reach 1000 k.

**Figure 9.** The reaction energy of decomposition paths with temperature.

All kinds of free radicals generated by ionization or dissociation of c-C₄F₈ molecules can produce a series of new products by secondary reactions, mainly CF₄, C₂F₆, C₃F₈, C₂F₄ and C₃F₆. Figure 10 shows the molecular model of the above decomposition product after optimization, and the bond length bond angle parameter is basically the same as that given in [30].

Table 4 shows the chemical equations of decomposition products, energy changes and activation energy. Among them, the processes of free radical recombination are exothermic reactions to generate CF₄, C₃F₈, C₂F₄, C₃F₆ and C₂F₆. From a thermodynamic point of view, CF₄, C₂F₆, C₂F₄ are relatively easy to form, and C₃F₈ generation is more difficult.

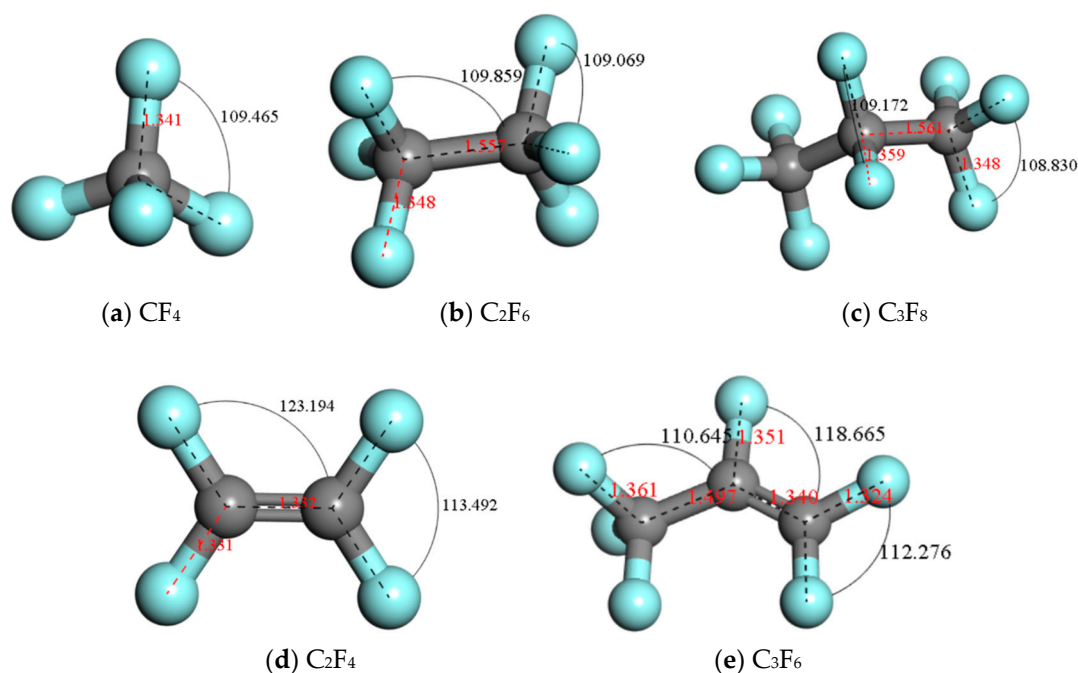


Figure 10. Molecular model of decomposition products and structural parameters.

Table 4. Decomposition products and energy change.

No	Chemical Equation	Energy Changes (kJ·mol ⁻¹)	Activation Energy (kJ·mol ⁻¹)
B1	CF ₂ · + F· → CF ₃ ·	-307.37	—
B2	C ₃ F ₆ · + 2F· → C ₃ F ₈	-83.7318	—
B3	CF ₃ · + F· → CF ₄	-190.262	—
B4	2CF ₂ · → C ₂ F ₄	-332.313	—
B5	2CF ₃ · → C ₂ F ₆	-373.811	—
B6	C ₃ F ₆ · → C ₃ F ₆	-81.21444	80.97188

According to the kinetic analysis, the path B1 to B5 reaction without energy barrier, are the processes of free radical complex into molecules, without activation spontaneously. The formation process of C₂F₆ release more energy, and the reaction is more prone to occur. The path B2 needs to release 83.7318 kJ/mol, which is the most difficult to occur with the least energy. Figure 11 shows the energy changes of reactions with temperature. With the increase of temperature, the absolute value of the reaction enthalpy showed a different degree of decline. That is, the temperature is conducive to the reaction.

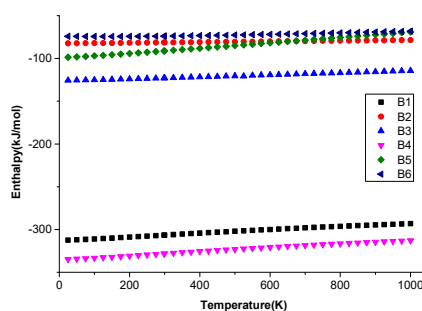


Figure 11. The energy changes of reactions with temperature.

Path B6 reaction requires the formation of an activated complex transition state (TS). The reactant absorbs energy of 80.97188 kJ/mol, and then the activated complex TS releases energy to form the final product. The progress of the reaction is shown in Figure 12. Small molecule product formation process

releases more energy, so it can be concluded that free radicals such as $F\cdot$, $CF_2\cdot$, $CF_3\cdot$ generated by the decomposition of $c-C_4F_8$ molecules tend to recombine into small molecules, resulting in a large content of small molecule products, which is in good agreement with the previous experimental results.

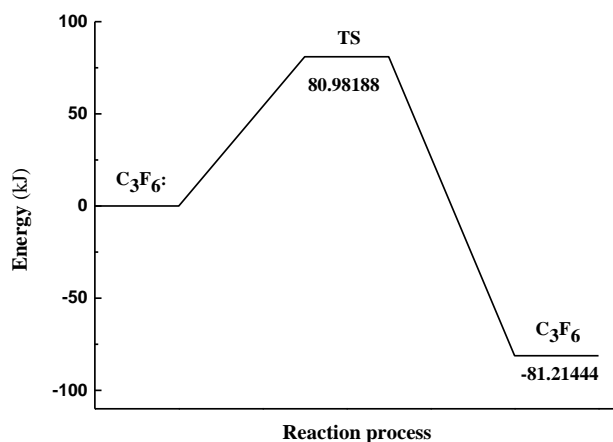


Figure 12. Reaction process of pathway B6 (TS: transition state).

In order to study the effect of O_2 on the decomposition of $c-C_4F_8$, the discharge decomposition path of O_2 must be studied first. In [20], the main pathways for generating $O\cdot$ are given by $O_2 \rightarrow 2O\cdot$ and $O_2 + e \rightarrow O\cdot + O$. It is also pointed out that the free radicals $CF_2\cdot$ and C_2F_4 are oxidized to COF_2 under O_2 conditions. Figure 12 shows the geometrically optimized COF_2 molecular structure model. Table 5 shows the reaction equations and energy changes for the free radical binding to COF_2 produced by $c-C_4F_8$ [20]. The reaction is an exothermic reaction. O_2 can oxidize $CF_2\cdot$ to form COF_2 and $O\cdot$ oxidize C_2F_4 to generate COF_2 and $CF_2\cdot$. The structure of COF_2 is shown in Figure 13.

Table 5. Reaction path and energy change.

No	Chemical Equation	Energy Changes ($kJ \cdot mol^{-1}$)	Activation Energy ($kJ \cdot mol^{-1}$)
C1	$CF_2\cdot + O_2 \rightarrow COF_2 + O\cdot$	-138.52	180.18
C2	$C_2F_4\cdot + O\cdot \rightarrow COF_2 + CF_2\cdot$	-112.64	184.61

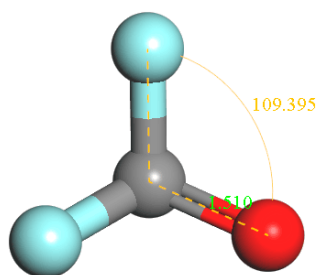


Figure 13. COF_2 molecular structure model.

4.3. The Basic Properties of the Main Products

According to the experimental measurement and calculation results, it can be seen that the main decomposition products are CF_4 , C_2F_4 , C_2F_6 , C_3F_6 and C_3F_8 , and COF_2 is produced when O_2 is involved. Figure 14 shows the molecular orbital energies of the main product. Based on the molecular orbital gap value, the main decomposition products have good stability. The C_2F_4 , C_3F_6 and COF_2 containing double bonds are poorly stable in the chemical reaction.

At the same time, the relative insulation properties of the decomposition products were compared. The environmental values and ecological toxicity are shown in Table 6.

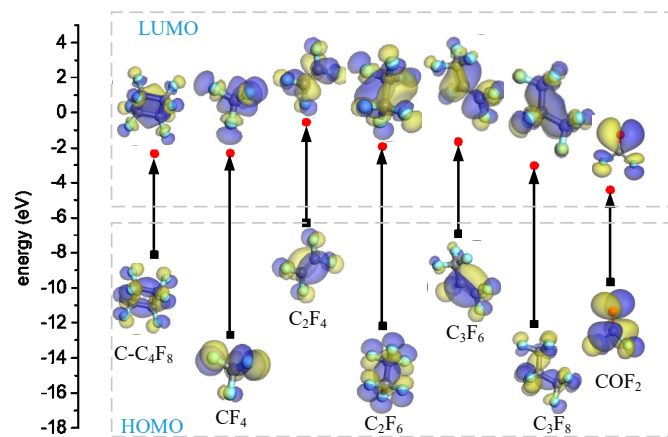


Figure 14. Molecular orbital gap values of decomposition products.

Table 6. Parameters of decomposition products.

Gas	Dielectric Strength Relative to SF ₆ [33–36]	Boiling Point (°C) [29–37]	GWP (100-Year) [5,36]	Lifetime (Year) [36–39]	Acute Toxicity
SF ₆	1	−63	23,900	3200	>500,000 ppm/4 h, LC50
c-C ₄ F ₈	1.12	−6	8700	2600	78 pph/2 h, LCLo
CF ₄	0.39	−186.8	6300	50,000	895,000 ppm/15 min, LCLo
C ₂ F ₆	0.78–0.79	−78	9200	10,000	>20 pph/2 h, LC
C ₃ F ₈	0.96–0.97	−37	7000	2600	750 ppm/4 h, LC50
C ₃ F ₆	—	−28	—	<10	750 ppm/4 h, LC50
C ₂ F ₄	—	−76.3	0	1.9 days	40,000 ppm/4 h, LC50
COF ₂	—	−84	0	—	270 mg/m ³ , 4 h, LC50

Note: GWP—global warming potential; LCLo—Lowest published lethal concentration; LC50—Lethal concentration, 50 percent kill; LC—Lethal concentration; The measurement of acute toxicity in the table is the test value of rat inhalation.

The insulation strength of CF₄ gas is about 39% of that of SF₆ and the insulation performance of C₂F₆ is about 76% of that of SF₆. The insulation performance of C₃F₈ is close to that of SF₆, and the C₄F₁₀ has better insulation performance than SF₆. The resulting decomposition products basically maintain the original mixed gas insulation properties. The GWP of all the products are lower than that of SF₆, and the concentration of the product is very small, so the product could be considered as not harmful to the environment. However, when oxygen is involved in the mixed gas discharge process, COF₂ will be generated, which is toxic and corrosive and harmful to the insulation equipment and operators. Therefore, oxygen content should be strictly controlled in the equipment.

5. Conclusions

- (1) During the breakdown process of the c-C₄F₈/N₂ mixed with O₂ included, a large amount of black powdery substance precipitates on the surface of the ball electrode, which are mainly composed of C, O, F, and O element content accounted for 17.32%.
- (2) The main products produced by c-C₄F₈ discharge decomposition are CF₄, C₂F₄, C₂F₆, C₃F₆ and C₃F₈ and small molecules such as CF₄, C₂F₄ and C₂F₆ are generated more easily. The addition of N₂ weakened the decomposition of c-C₄F₈ gas. The decomposition products mainly come from c-C₄F₈ and N₂ in the mixed gas does not participate in the chemical reaction. The product has good insulation properties. The presence of O₂ causes the promotion of c-C₄F₈ decomposition and produces COF₂. The increase of temperature can promote the reaction.
- (3) The main products produced by c-C₄F₈ discharge have good insulation properties, and the products basically maintain the insulation properties of the original mixed gas. However, when O₂ was involved, COF₂ gas was detected, which is toxic and corrosive and would be hazardous to insulation equipment and operators.

In summary, $c\text{-C}_4\text{F}_8$ should not be mixed with dry air. In order to ensure the safe and reliable operation of equipment, the oxygen content in the $c\text{-C}_4\text{F}_8$ mixed gas should be strictly controlled.

Author Contributions: Conceptualization, S.T. and S.X.; Methodology, S.T.; Software, Z.D.; Validation, Y.C.; Writing-Original Draft Preparation, S.T.; Writing-Review and Editing, S.T.; Visualization, Y.L.; Supervision, X.Z.; Project Administration, J.T.

Funding: This work is supported by the Natural Science Foundation of China (Program No. 51707137) and China Postdoctoral Science Foundation Grant (Program No. 2017M612502).

Conflicts of Interest: The authors declare no conflict of interest.

References

1. Tsai, W.-T. The decomposition products of sulfur hexafluoride (SF₆): Reviews of environmental and health risk analysis. *J. Fluor. Chem.* **2007**, *128*, 1345–1352. [[CrossRef](#)]
2. Reilly, J.; Prinn, R.; Harnisch, J.; Fitzmaurice, J.; Jacoby, H.; Kicklighter, D.; Melillo, J.; Stone, P.; Sokolov, A.; Wang, C. Multi-gas assessment of the Kyoto Protocol. *Nature* **1999**, *401*, 549–555. [[CrossRef](#)]
3. Zhang, X.; Li, Y.; Tian, S.; Xiao, S.; Chen, D.; Tang, J.; Zhou, R. Decomposition mechanism of the C₅-PFK/CO₂ gas mixture as an alternative gas for SF₆. *Chem. Eng. J.* **2018**, *336*, 38–46. [[CrossRef](#)]
4. Lindley, A.A.; McCulloch, A. Regulating to reduce emissions of fluorinated greenhouse gases. *J. Fluor. Chem.* **2005**, *126*, 1457–1462. [[CrossRef](#)]
5. Ravishankara, A.R.; Solomon, S.; Turnipseed, A.A.; Warren, R.F. Atmospheric lifetimes of long-lived halogenated species. *Science* **1993**, *259*, 194–199. [[CrossRef](#)] [[PubMed](#)]
6. Kieffel, Y.; Irwin, T.; Ponchon, P.; Owens, J. Green gas to replace SF₆ in electrical grids. *IEEE Power Energy Mag.* **2016**, *14*, 32–39. [[CrossRef](#)]
7. Mota-Babiloni, A.; Navarro-Esbrí, J.; Barragán-Cervera, Á.; Molés, F.; Peris, B. Analysis based on EU Regulation No 517/2014 of new HFC/HFO mixtures as alternatives of high GWP refrigerants in refrigeration and HVAC systems. *Int. J. Refrig.* **2015**, *52*, 21–31. [[CrossRef](#)]
8. Zhang, X.; Xiao, H.; Tang, J.; Cui, Z.; Zhang, Y. Recent advances in decomposition of the most potent greenhouse gas SF₆. *Crit. Rev. Environ. Sci. Technol.* **2017**, *47*, 1763–1782. [[CrossRef](#)]
9. Vijk, A.K. The nature of metal-electrodes/SF₆ reactions in SF₆ decomposition due to direct-current interruption under simulated circuit-breaker conditions. *IEEE Trans. Electr. Insul.* **1976**, *EI-11*, 157–160. [[CrossRef](#)]
10. Wock, S. On the toxicity of SF₆ insulating gas. *IEEE Trans. Electr. Insul.* **1984**, *EI-19*, 156. [[CrossRef](#)]
11. Mitchell, A.D. *Genetic Toxicity Evaluation of Iodotrifluoromethane (CF₃I). Volume I: Results of Salmonella Typhimurium Histidine Reversion Assay (Ames Assay)*; Genesys Research Inc.: Research Triangle Park, NC, USA, 1995.
12. Zhang, X.; Xiao, S.; Han, Y.; Dai, Q. Analysis of the feasibility of CF₃I/CO₂ used in C-GIS by partial discharge inception voltages in positive half cycle and breakdown voltages. *IEEE Trans. Dielectr. Electr. Insul.* **2015**, *22*, 3234–3243. [[CrossRef](#)]
13. Hyrenbach, M.; Hintzen, T.; Müller, P.; Owens, J. Alternative gas insulation in medium-voltage switchgear. In Proceedings of the 23rd International Conference on Electricity Distribution, Lyon, France, 15–18 June 2015.
14. Andersen, M.P.S.; Kyte, M.; Andersen, S.T.; Nielsen, C.J.; Nielsen, O.J. Atmospheric chemistry of (CF₃)₂CF–CN: A replacement compound for the most potent industrial greenhouse gas, SF₆. *Environ. Sci. Technol.* **2017**, *51*, 1321–1329. [[CrossRef](#)] [[PubMed](#)]
15. Li, Y.; Zhang, X.; Xiao, S.; Chen, Q.; Tang, J.; Chen, D.; Wang, D. Decomposition properties of C₄F₇N/N₂ gas mixture: An environmentally friendly gas to replace SF₆. *Ind. Eng. Chem. Res.* **2018**, *57*, 5173–5182. [[CrossRef](#)]
16. Zhao, H.; Li, X.; Lin, H. Insulation characteristics of $c\text{-C}_4\text{F}_8\text{-N}_2$ and CF₃I-N₂ mixtures as possible substitutes for SF₆. *IEEE Trans. Power Deliv.* **2017**, *32*, 254–262. [[CrossRef](#)]
17. Kang, L.; Wenhao, N.; Guoqiang, Z.; Haijiang, X. Investigation of voltage and potential gradient of arc column in fluorocarbon gas and its gas mixtures. In Proceedings of the 2013 IEEE International Conference on Electrical Machines and Systems (ICEMS), Busan, Korea, 26–29 October 2013; pp. 2255–2258.

18. Liu, X.; Wang, J.; Wang, Y.; Zhang, Z.; Xiao, D. Analysis of the insulation characteristics of c-C₄F₈/CO₂ gas mixtures by the Monte Carlo method. *J. Phys. D Appl. Phys.* **2007**, *41*, 015206. [[CrossRef](#)]
19. Christophorou, L.G.; Olthoff, J.K.; Green, D.S. *Gases for Electrical Insulation and Arc Interruption: Possible Present and Future Alternatives to Pure SF₆*; Technical Note (NIST TN)-1425; NIST: Gaithersburg, MD, USA, 1997.
20. Li, X.; Zhao, H.; Jia, S.; Murphy, A.B. Prediction of the dielectric strength for c-C₄F₈ mixtures with CF₄, CO₂, N₂, O₂ and air by Boltzmann equation analysis. *J. Phys. D Appl. Phys.* **2014**, *47*, 425204. [[CrossRef](#)]
21. Kang, L.; Wenhao, N.; Tao, L.; Guoqiang, Z.; Haijiang, X. Study of the decomposition of c-C₄F₈ and its mixture with N₂ under 50 Hz ac corona discharge. In Proceedings of the Electrical Insulation and Dielectric Phenomena (CEIDP), Shenzhen, China, 20–23 October 2013; pp. 1229–1232.
22. Hayashi, T.; Ishikawa, K.; Sekine, M.; Hori, M.; Kono, A.; Suu, K. Dissociation channels of c-C₄F₈ to CF₂ radical in reactive plasma. *Jpn. J. Appl. Phys.* **2011**, *50*, 036203. [[CrossRef](#)]
23. Graber, L. Improving the accuracy of SF₆ leakage detection for high voltage switchgear. *IEEE Trans. Dielectr. Electr. Insul.* **2011**, *18*, 1835–1846. [[CrossRef](#)]
24. Yamamoto, O.; Takuma, T.; Hamada, S.; Yamakawa, Y.; Yashima, M. Applying a gas mixtures containing c-C₄F₈ as an insulation medium. *IEEE Trans. Dielectr. Electr. Insul.* **2001**, *8*, 1075–1081. [[CrossRef](#)]
25. Navarrini, W.; Venturini, F.; Tortelli, V.; Basak, S.; Pimparkar, K.P.; Adamo, A.; Jensen, K.F. Direct fluorination of carbon monoxide in microreactors. *J. Fluor. Chem.* **2012**, *142*, 19–23. [[CrossRef](#)]
26. Chu, F.Y. SF₆ decomposition in gas-insulated equipment. *IEEE Trans. Electr. Insul.* **1986**, *EI-21*, 693–725. [[CrossRef](#)]
27. Tang, J.; Liu, F.; Zhang, X.; Meng, Q.; Zhou, J. Partial discharge recognition through an analysis of SF₆ decomposition products part 1: Decomposition characteristics of SF₆ under four different partial discharges. *IEEE Trans. Dielectr. Electr. Insul.* **2012**, *19*, 29–36. [[CrossRef](#)]
28. Tang, J.; Yang, D.; Zeng, F.; Tang, B.; Li, K.; Yao, Q.; Miao, Y. Correlation characteristics between gas pressure and SF₆ decomposition under negative DC partial discharge. *IET Gener. Transm. Distrib.* **2017**, *12*, 1240–1246. [[CrossRef](#)]
29. Liu, C.; Palanisamy, S.; Chen, S.; Wu, P.; Yao, L.; Lou, B.S. Mechanism of formation of SF₆ decomposition gas products and its identification by GC-MS and electrochemical methods: A mini Review. *Int. J. Electrochem. Sci.* **2015**, *10*, 4223–4231.
30. Zhang, X.; Tian, S.; Xiao, S.; Deng, Z.; Li, Y.; Tang, J. Insulation strength and decomposition characteristics of a C₆F₁₂O and N₂ gas mixture. *Energies* **2017**, *10*, 1170. [[CrossRef](#)]
31. Xiao, S.; Li, Y.; Zhang, X.; Tang, J.; Tian, S.; Deng, Z. Formation mechanism of CF₃I discharge components and effect of oxygen on decomposition. *J. Phys. D Appl. Phys.* **2017**, *50*, 155601. [[CrossRef](#)]
32. Perdew, J.P.; Wang, Y. Accurate and simple analytic representation of the electron-gas correlation energy. *Phys. Rev. B Condens. Matter* **1992**, *45*, 13244. [[CrossRef](#)] [[PubMed](#)]
33. Wada, J.; Ueta, G.; Okabe, S.; Hikita, M. Dielectric properties of gas mixtures with per-fluorocarbon gas and gas with low liquefaction temperature. *IEEE Trans. Dielectr. Electr. Insul.* **2016**, *23*, 838–847. [[CrossRef](#)]
34. Devins, J.C. Replacement gases for SF₆. *IEEE Trans. Electr. Insul.* **1980**, *EI-15*, 81–86. [[CrossRef](#)]
35. Deng, Y.; Xiao, D. Analysis of the insulation characteristics of CF₃I gas mixtures with Ar, Xe, He, N₂, and CO₂ using Boltzmann equation method. *Jpn. J. Appl. Phys.* **2014**, *53*, 096201. [[CrossRef](#)]
36. Takahashi, K.; Itoh, A.; Nakamura, T.; Tachibana, K. Radical kinetics for polymer film deposition in fluorocarbon (C₄F₈, C₃F₆, and C₅F₈) plasmas. *Thin Solid Films* **2000**, *374*, 303–310. [[CrossRef](#)]
37. Ivy, D.J.; Rigby, M.; Baasandorj, M.; Burkholder, J.B.; Prinn, R.G. Global emission estimates and radiative impact of C₄F₁₀, C₅F₁₂, C₆F₁₄, C₇F₁₆ and C₈F₁₈. *Atmos. Chem. Phys.* **2012**, *12*, 7635–7645. [[CrossRef](#)]
38. Surhone, L.M.; Timpledon, M.T.; Marseken, S.F. Novec 1230. *Landolt Börnstein Group IV Phys. Chem.* **2010**, *26*, 263–291.
39. Eden, S.; Limão-Vieira, P.; Kendall, P.A.; Mason, N.J.; Delwiche, J.; Hubin-Franskin, M.J.; Tanaka, T.; Kitajima, M.; Tanaka, H.; Cho, H.; et al. Electronic excitation of tetrafluoroethylene, C₂F₄. *Chem. Phys.* **2004**, *297*, 257–269. [[CrossRef](#)]

